First-principles study of the structural and elastic properties of rhenium-based transition-metal alloys

Maarten de Jong,[1,*] David L. Olmsted,[1] Axel van de Walle,[2] and Mark Asta[1]
[1]*Department of Materials Science and Engineering, University of California, Berkeley, California 94720, USA*
[2]*School of Engineering, Brown University, Providence, Rhode Island 02912, USA*
(Received 22 September 2012; published 5 December 2012)

Structural, energetic, and elastic properties of hexagonal-close-packed rhenium-based transition-metal alloys are computed by density-functional theory. The practical interest in these materials stems from the attractive combination of mechanical properties displayed by rhenium for structural applications requiring the combination of high melting temperature and low-temperature ductility. Single-crystal elastic constants, atomic volumes, axial c/a ratios, and dilute heats of solution for Re-X alloys are computed, considering all possible transition-metal solute species X. Calculated elastic constants are used to compute values of a commonly considered intrinsic-ductility parameter K/G, where K is the bulk modulus and G denotes the Voigt average of the shear modulus, as well as the anisotropies in the Young's modulus and shear modulus. The calculated properties show clear trends as a function of d-band filling, which can be rationalized through tight-binding theory. The results indicate that solutes to the left of rhenium in the periodic table show a tendency to increase the intrinsic ductility parameter, a trend that correlates with an increase of the c/a ratio towards the ideal value associated optimal close packing. The Young's modulus shows a trend towards increasing isotropy with alloying of solutes X to the left of Re, while the shear modulus shows the opposite trend but with an overall weaker dependence on solute additions.

DOI: 10.1103/PhysRevB.86.224101 PACS number(s): 62.20.fk, 62.20.de, 31.15.ae, 61.72.Bb

I. INTRODUCTION

Among the refractory elements, Re is unique in displaying a hexagonal-close-packed (HCP) crystal structure, as opposed to the body-centered-cubic structure shared by Nb, Mo, Ta, and W. This difference in crystal structure correlates with the fact that Re is known to be the only refractory element that does not display a measured ductile-brittle transition, such that it features relatively high ductility at low temperature.[1,2] The combination of low-temperature ductility and high melting point make Re-based alloys attractive as structural materials for high-temperature applications. However, the exceptionally high cost and limited worldwide reserves of elemental Re have resulted in limited use of such alloys to date.[3,4] There is thus practical interest in finding replacement strategies for Re, with one approach being the identification of solute atoms that can be added to Re in high concentrations without significantly altering its desirable mechanical properties. For such a strategy to be effective, solute atoms must be identified that, at a minimum, maintain the high melting temperature of Re without compromising low-temperature ductility.

To aid in such alloy design efforts, it is useful to understand the effect on intrinsic structural and elastic properties resulting from substitutional alloying (e.g., Ref. 5). Here we focus on alloying with transition-metal (TM) solutes, as it is expected that combinations of these elements chosen to maintain a d-band filling close to that characteristic of Re could be effective in retaining high melting temperatures, due to the well-known maximum in the cohesive energy that occurs at approximately half d-band filling.[6–8] We thus consider HCP Re-X alloys, with all possible $3d$, $4d$, and $5d$ solute elements X, and calculate by density-functional theory (DFT) three classes of properties: dilute heats of mixing, single-crystal elastic constants, and structural properties including atomic volume and axial c/a ratio. Since one of the main attractive features of Re is its low-temperature ductility, we use these DFT results also to study trends in the effects of TM solutes on properties that are expected to correlate with this property.

Several approaches have been proposed in the literature to examine the intrinsic ductility of a material from first-principles DFT calculations.[9–15] The simplest approach is based on the consideration of a ductility parameter $D = K/G$, defined as the ratio of the bulk modulus (K) to the Voigt average of the shear modulus (G). In HCP metals, this parameter has been shown to correlate well with the relative ductility,[9,12] with a higher K/G ratio indicating a tendency towards enhanced ductility. This correlation can be understood simply from a picture where microcrack initiation and propagation requires bond breaking, which becomes more difficult for high values of the bulk modulus, K, while deformation mechanisms that give rise to plasticity are expected to be more prevalent in materials with comparatively low shear moduli G.

A second property that can be expected to affect ductility in polycrystalline samples is the crystalline anisotropy of the elastic constants. Specifically, for systems with highly anisotropic elastic constants, applied loads can lead to stress concentrations at grain boundaries and triple junctions that can contribute to brittle failure.[16–18] From this standpoint, it is expected that a lower degree of elastic anisotropy should contribute to an enhancement in the ductility of polycrystalline materials. We thus consider the effect of solute additions on elastic anisotropy in Re-based TM alloys, using as a measure of the crystalline anisotropy two parameters introduced recently in Ref. 19, measuring the anisotropy in the Young's and shear modulus, respectively.

More sophisticated models have been developed for analyzing ductility by DFT, where the energetic competition between the creation of fresh surface (brittle behavior) versus the formation of twins or stacking faults (ductile behavior) is considered.[9–13] For HCP metals, such models consider the energetics of surface formation relative to slip

on basal and prismatic planes and twinning on the $\{11\bar{2}1\}$ planes, which are known to constitute important deformation mechanisms.[9,13,20–22] Since the emphasis of the present work is on the study of general trends in the intrinsic ductility induced by the addition of TM solute atoms in HCP Re, we will focus specifically on the consideration of the parameter K/G, leaving the investigation of more detailed theoretical models for future work focused on a more limited set of promising compositions.

The remainder of this paper is organized as follows. In the next section we give the computational details, including the DFT methodology, the calculations of single-crystal elastic constants, and the supercell modeling of alloys. The results are presented in Sec. III, where we first compare results for elemental Re with previous calculations and experimental measurements. The trends in calculated properties with d-band filling are then presented. A discussion of these trends in the context of tight-binding theories is presented in Sec. IV. The last section summarizes the main conclusions in the context of the design of Re alloys outlined above.

II. METHODOLOGY

A. DFT Calculations

All of the DFT results presented in this work were performed using the projector augmented wave (PAW) method,[23,24] as implemented in the Vienna *Ab Initio* Simulation Package (VASP).[25,26] In these calculations use was made of the Perdew-Zunger parametrization of the Ceperly-Alder[27,28] exchange-correlation energy within the local density approximation (LDA-CA).

An energy cutoff for the plane wave basis set of 450 eV was used. Brillouin zone integrations were performed using Monkhorst-Pack k-point sampling;[29] in all the total energy calculations, the density of k points is chosen such that the number of k points in the first Brillouin zone times the number of atoms in the cell was approximately 15000. Occupation of the electronic states was performed using the Methfessel-Paxton scheme,[30] with a smearing width of 0.1 eV. For the structural optimizations, internal coordinates were relaxed until the atomic forces converged to within 0.001 eV/Å. The equilibrium lattice parameters were computed using a conjugate-gradient minimization algorithm, employing the calculated stress tensors. In all calculations, the residual stresses, after the full relaxation, did not exceed 0.05 kBar (5 MPa).

The PAW potential used for Re corresponds to the electron configuration $5d^5 6s^2$, with seven electrons treated explicitly as valence. For all solutes, PAW potentials corresponding to the nominal valence electrons were employed. For Re and the alloy supercells (see below) the results presented, were obtained using nonmagnetic calculations. For solute species Fe, Co, Ni, Cr, and Mn spin polarization was considered although nonmagnetic states were obtained upon structural relaxation. In calculations of the dilute heats of solution, the reference energies for elemental Cr, Mn, Fe, Co, or Ni were also performed employing spin-polarized calculations; for Fe, Co and Ni a ferromagnetic ground state was obtained, while for Cr and Mn, the relaxed structured converged to nonmagnetic solutions.

B. Elastic constant calculations

The calculation of the elastic constants was performed using as a starting point the relaxed structures obtained from the calculations described in the previous subsection. For each such structure 24 unique deformation mappings are constructed, corresponding to six independent deformation modes. In the first set, ε_{11}, ε_{22}, and ε_{33} corresponds to the uniaxial deformations whereas in the second, ε_{12},ε_{23},ε_{13} corresponds to the simple shear deformations. For calculating the elastic constants, four values for the strain $(-\varepsilon_0, -\frac{1}{2}\varepsilon_0, +\frac{1}{2}\varepsilon_0, +\varepsilon_0)$ were applied for each of the six deformation modes. For uniaxial deformation, we used $\varepsilon_0 = 0.01$ and for simple shear $\varepsilon_0 = 0.004$. Each of the deformations is characterized by a deformation gradient tensor $\mathbf{F}$. The Green-Lagrange strain tensor $\mathbf{E}$ (which reduces to the linear strain tensor for small strains) is calculated according to Eq. (1),

$$\mathbf{E} = \tfrac{1}{2}(\mathbf{F}^{\mathrm{T}}\mathbf{F} - \mathbf{I}). \tag{1}$$

The components of the Cartesian stress tensor are calculated from first principles, while allowing for ionic relaxations. Subsequently, all components of the elastic tensor can be determined by a least-squares fit of the calculated stresses to the applied Green-Lagrange strain. This means every elastic constant is fit to a total of five points, including the fully relaxed (zero stress, zero strain) configuration.

Several tests were performed to estimate the numerical precision of the calculated elastic constants. In the first set of tests we considered the convergence with respect to k points and plane wave energy cutoff, giving an estimated precision of about 9.5 GPa for all elastic moduli presented below. Further, the fitting procedure for the elastic constants was examined to test the assumption of linear stress-strain relations. Specifically, we compared the results obtained for the range of deformations given above to values obtained by fitting to a more limited range of strains: $(-\varepsilon_0, 0, +\varepsilon_0)$. It was found that the consideration of this more limited range of strains led to very similar results for the elastic constants, differing by less than 1.5 GPa, compared to the values obtained from the expanded range of strains given above. A final check of the accuracy of the elastic constants was performed by comparing the symmetry of the calculated elastic tensor to the theoretical symmetry, as dictated by the HCP structure. To this end, the calculated elastic tensor is projected onto the closest fourth-order elastic tensor exhibiting HCP symmetry. This method[31–33] effectively minimizes the Euclidean distance between the calculated elastic tensor and the tensor on which the calculated elastic tensor is projected. For the first-principles parameters used in this study, we found that all components of the calculated elastic tensor were converged to within 2.6 GPa of the closest tensor exhibiting the underlying HCP symmetry.

For the calculation of the ductility parameter K/G the bulk modulus K is determined from the calculated single-crystal elastic constants through the relation[34]

$$K = \frac{2(C_{11} + C_{12}) + 4C_{13} + C_{33}}{9}. \tag{2}$$

The Voigt average of the shear modulus G is calculated from the single-crystal elastic constants using the following expression:[34]

$$G = \frac{(C_{11} + C_{33} - 2C_{13} - C_{66})/3 + 2C_{44} + 2C_{66}}{5}. \quad (3)$$

From the convergence tests described above, the numerical precision of the calculated values of K/G is estimated to be within about 2% of the values given below.

To investigate the degree of elastic anisotropy we make use of two parameters, f_E and f_G, introduced in Ref. 19. These parameters measure respectively the anisotropy of the Young's modulus and shear modulus, and are defined in terms of the elastic compliances (S_{ij}), as follows:

$$f_E = S_{11}/S_{33} \quad (4)$$

$$f_G = (S_{44} + 2S_{11} - 2S_{12})/2S_{44}. \quad (5)$$

Values of f_E and f_G equal to one correspond to elastically isotropic solids, while deviations from unity provide a measure of elastic anisotropy.

C. Supercell models for alloys

To study the effects of alloying Re with $3d$, $4d$, and $5d$ TM solutes, we employ a 2×2×2 HCP supercell containing 16 total atoms. A single Re atom is substituted by a TM atom X, yielding composition $Re_{15}X_1$. For each such supercell, structural relaxations were performed, and the results used to compute three quantities: the solute expansion coefficients η_a and η_c, and the heat of solution ΔH_{sol}. The latter quantity is computed as follows:

$$\Delta H_{sol} = E(Re_{15}X_1) - 15E(Re) - E(X), \quad (6)$$

where $E(Re_{15}X)$ is the energy of the $Re_{15}X$ supercell, while $E(Re)$ and $E(X)$ denote the energies per atom of pure Re and X in their relaxed equilibrium crystal structures, respectively. The solute expansion coefficients are computed as

$$\eta_a \equiv \partial \ln(a)/\partial x \approx 16\,[a(Re_{15}X_1) - a(Re)]\,/a(Re) \quad (7)$$

$$\eta_c \equiv \partial \ln(c)/\partial x \approx 16\,[c(Re_{15}X_1) - c(Re)]\,/c(Re), \quad (8)$$

where x denotes the mole fraction of the solute, $a(Re_{15}X_1)$ and $c(Re_{15}X_1)$ denote the lattice parameters derived from the relaxed 16-atom supercell, and $a(Re)$ and $c(Re)$ correspond to the lattice parameters for pure Re. The relaxed supercells are also used as the starting point for calculations of the single-crystal elastic constants, following the procedure described in the previous subsection.

III. RESULTS

In this section we present the results of calculated structural, energetic and elastic properties for pure Re and Re-X transition-metal alloys and compare to previously published computational and experimental results. Each of the calculated properties for the alloys considered in this work is shown to display clear trends with the number of d electrons in the TM solutes. These trends are discussed in the context of canonical d-band theory in the next section.

A. Structural and elastic properties of pure rhenium

In Table I the values of the structural parameters and elastic moduli computed in the present work for elemental Re are compared to results from previous computational studies and experimental measurements. Considering first the comparison between our results and experiments, we see that the calculated a and c lattice constants are underestimated by approximately 0.7%, while the elastic moduli are overestimated by approximately 8%, except for C_{13}, which shows a larger disagreement with experiments of about 20%. This level of agreement is viewed to be reasonable given that the present calculations made use of the LDA, which generally shows a tendency to overbind. We note, however, that the only other previous calculation that made use of the LDA-CA exchange-correlation potential[35] shows slightly better agreement with experiment for a and c lattice parameters, while the values of C_{11}, C_{33}, and C_{44} are considerably larger that those obtained in the current work and all other previous calculations listed in Table I.

By contrast, the two other sets of LDA results[36,37] listed in Table I feature elastic moduli that are on average 6% and 16% smaller than the values calculated in the present work, and closer to experimental measurements. The differences with the present results may be due to the different parametrizations of the LDA used in these previous calculations: the work in Refs. 36 and 37 made use of the Vosko, Wilk, and Nusair (VWN)[38] and Hedin-Lundqvist (HL)[39] parametrizations of LDA, respectively. The calculated results listed in Table I[36,37] obtained with the generalized-gradient approximation of Perdew *et al.*[40] (GGA-PBE) show the expected trend featuring larger lattice parameters and smaller elastic moduli, relative to the present LDA-CA results.

Overall, the best level of agreement between experiment and theory appears to be obtained from the GGA-PBE results of Ref. 37. In what follows we will focus on the changes in structural and elastic properties associated with the addition of TM solutes to HCP Re, and the trends that these changes display as a function of band filling. For this purpose, the slightly lower accuracy of the LDA-CA exchange correlation is not expected to affect the main conclusions of the work. Moreover, since much of this work involves investigating dimensionless alloy parameters such as the ductility parameter K/G, it is expected that systematic biases between GGA and LDA will not affect the overall results strongly.

B. Structural properties of Re-based transition metal alloys

Table II lists the calculated values of the solute expansion coefficients [$\eta_a = \partial \ln a)/\partial x$ and $\eta_c = \partial \ln(c)/\partial x$] for each of the $3d$, $4d$, and $5d$ solutes X considered. Trends in associated structural properties are plotted as a function of the number of d electrons for the solute species in Figs. 1 and 2.

Figure 1 plots the volume expansion coefficient $\eta_V = \partial \ln(V)/\partial x = 2\eta_a + \eta_c$ as a function solute d-band filling. A nearly parabolic trend is observed for each of the $3d$, $4d$, and $5d$ series, with minima corresponding to the Co/Rh/Ir column. All of the $3d$ solutes except Sc and Ti lead to a decrease in molar volume, with the most negative values corresponding to Co. The values for the $4d$ and $5d$ elements are comparable;

TABLE I. Structural and elastic properties of HCP Re, based on the computational and experimental (Exp.) methods listed in the first column. The units for the reported values of lattice constants (a and c), atomic volume (Ω), and elastic moduli (C_{ij}) are Å, Å^3, and GPa, respectively. For the lattice parameters and atomic volume, experimental values extrapolated to zero temperature, using reported thermal expansion coefficients, are given in parentheses.

Method	a	c	c/a	Ω	C_{11}	C_{33}	C_{12}	C_{13}	C_{44}	K/G	f_E	f_G
NCPP,[a] GGA-PBE[36]	2.762	4.442	1.608	14.67	607	705	307	209	164	2.14	1.40	1.05
NCPP, LDA-VWN[36]	2.756	4.437	1.61	14.58	623	731	327	218	170	2.18	1.45	1.07
FLMTO,[b] LDA-CA[42]	2.748	4.474	1.628	14.62	837	895	293	217	223	1.68	1.14	0.91
FLAPW,[c] LDA-HL[37]	2.750	4.442	1.615	14.54	605	650	235	195	175	1.83	1.14	0.97
FLAPW, GGA-PBE[37]	2.794	4.513	1.615	15.25	640	695	280	220	170	2.02	1.20	0.97
PAW, LDA-CA (this work)	2.741	4.422	1.613	14.39	672	740	309	252	176	2.16	1.18	0.98
Exp. (x-ray)[44]	2.762	4.455	1.613	14.71	×	×	×	×	×	×	×	×
	(2.756)	(4.448)	1.613	(14.63)	×	×	×	×	×	×	×	×
Exp. (x-ray)[45]	2.761	4.456	1.614	14.70	×	×	×	×	×	×	×	×
	(2.755)	(4.449)	1.614	(14.63)	×	×	×	×	×	×	×	×
Exp. (x-ray)[46]	×	×	×	×	619	687	278	204	162	2.02	1.25	0.98
Exp. (ultrasound)[47]	×	×	×	×	616	683	273	206	161	2.02	1.24	0.97

[a]Norm-conserving pseudopotential[41]
[b]Full potential linear muffin-tin orbital[35]
[c]Full potential linearized augmented planewave[43]

most of these solutes show positive values of η_V, with Tc, Ru/Os, Rh/Ir, Pd/Pt giving weakly negative values.

Figure 2 plots the axial c/a ratio of the 16-atom $Re_{15}X_1$ cells as a function of the solute d-band filling. In this case a general trend is observed for a decreasing value of c/a going from the left to the right in the d-band series. The trend is nearly monotonic, with some exceptions at the ends of the series on either side (La, Cd, and Hg). It is noteworthy that pure Re has a value of $c/a \approx 1.61$, which is roughly one percent lower the ideal value of $\sqrt{8/3} \approx 1.63$ corresponding to optimal close packing. Solutes to the left of Re in the periodic table are seen to increase c/a, making it closer to ideal, while those to the right of Re lower c/a.

Experimental data on the structural parameters of Re-based alloys is scarce and the effects of alloying with different solutes is not well established. However, for the binary systems Re-W, Re-Ir, and Re-Pt, our results regarding the trends in the structural parameters are consistent with those identified in some early experimental measurements.[48] In Ref. 48, the lattice parameters, c/a ratio and atomic volume of Re-based alloys were experimentally determined. Solute elements W, Ir, and Pt were added in concentrations between 5 and 40 at.% while maintaining the HCP phase. Consistent with the current work, Ir and Pt were found to decrease the c/a ratio whereas W leads to an increase. The trends in the variation of volume with band filling, as found in Ref. 48, are confirmed in the present work as well. Alloying with W is found to lead to a positive lattice expansion coefficient in elemental Re, whereas both Ir and Pt show negative lattice expansion coefficients. Pt is known experimentally[48] to exhibit positive volume expansion coefficients when added to Re in concentrations exceeding about 40 at.%. These observations cannot be compared to results from the present work in which much lower solute concentrations have been studied.

C. Energetics of Re-based transition metal alloys

The energetics of alloying is examined through consideration of the dilute heat of solution ΔH_{sol} defined in Eq. (6).

TABLE II. Calculated solute lattice expansion coefficients η_a and η_c and heat of solution ΔH_{sol} (kJ/mol solute) of solutes in rhenium remove this phrase as it is redundant with text in the main manuscript.

3d		Sc	Ti	V	Cr	Mn	Fe	Co	Ni	Cu	Zn
	η_a	0.047	−0.013	−0.050	−0.071	−0.081	−0.084	−0.086	−0.071	−0.038	−0.001
	η_c	0.186	0.098	0.011	−0.047	−0.089	−0.114	−0.118	−0.123	−0.119	−0.089
	ΔH_{sol}	100.7	17.6	37.4	64.9	28.6	3.9	−5.2	2.57	87.6	93.1
4d		Y	Zr	Nb	Mo	Tc	Ru	Rh	Pd	Ag	Cd
	η_a	0.117	0.073	0.024	0.004	−0.010	−0.011	−0.012	0.005	0.044	0.078
	η_c	0.373	0.277	0.164	0.062	−0.018	−0.063	−0.068	−0.058	−0.036	0.0236
	ΔH_{sol}	268.2	99.7	53.1	46.3	−1.8	−25.4	−58.3	−3.0	167.2	206.5
5d		La	Hf	Ta	W	Re	Os	Ir	Pt	Au	Hg
	η_a	0.184	0.052	0.020	0.001	0	0.001	0.005	0.020	0.055	0.092
	η_c	0.348	0.249	0.170	0.078	0	−0.048	−0.067	−0.057	−0.036	0.032
	ΔH_{sol}	403.9	54.2	35.2	47.2	0	−27.3	−85.5	−72.2	82.7	212.6

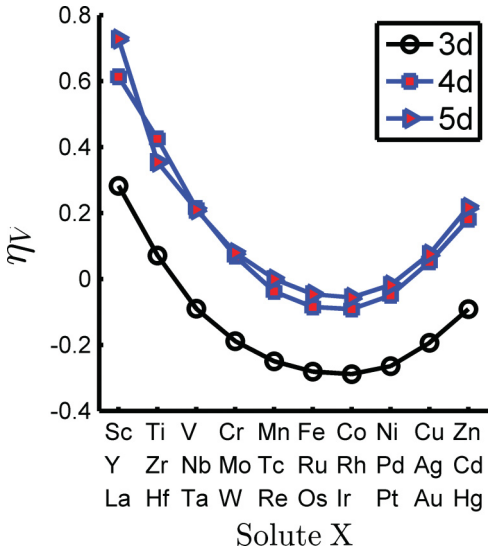

FIG. 1. (Color online) Volume solute expansion coefficient as a function of $3d$, $4d$, or $5d$ solute element for alloy composition $Re_{15}X_1$.

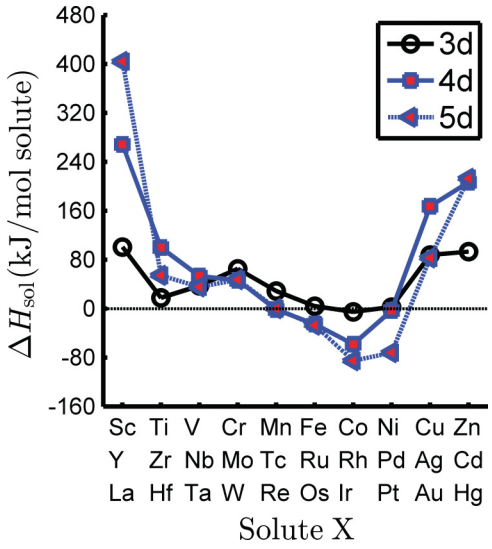

FIG. 3. (Color online) Heat of solution as a function of $3d$, $4d$, or $5d$ solute element for alloy composition $Re_{15}X_1$.

Results for this property are listed in Table II and plotted in Fig. 3. The heats of solution for the $3d$, $4d$, and $5d$ elements with 3 or $4d$ electrons (V, Nb, Ta, Cr, W, Mo) are weakly positive, while elements further to the left in the periodic table feature increasingly positive values. The $4d$ and $5d$ elements having 5, 6, or $7d$ electrons (Ru, Os, Rh, Ir, Pd, Pt) all yield negative heats of solution, whereas the corresponding $3d$ elements (Fe, Co, Ni) show weakly positive values. Moving further to the right in the periodic table, to elements with 8, 9, or $10d$ electrons, we observe again strongly positive heats of solution for all of the $3d$, $4d$, and $5d$ solutes.

Experimental data on the thermodynamics of Re-rich alloys is relatively scarce. However, the present results can be compared to recent related computational studies,[49,50] as well as free-energy models derived from phase-diagram assessments performed within the framework of the calculation of phase diagrams (CALPHAD) formalism.[51] To enable these comparisons, it is useful to consider the dilute heat of mixing ΔH_{mix}, which is defined analogously to Eq. (6) but with the $E(X)$ defined as the energy of element X in the HCP structure (rather than its lowest-energy structure if different than HCP). A negative value of ΔH_{mix} is indicative of an ordering tendency, such that the lowest-energy atomic configurations on the HCP parent structure would be expected to be ordered compounds. In the computational work reported in Refs. 49 and 50, Re-rich $D0_{19}$-prototype ground-state structures were identified with compositions Re_3Pd, Re_3Pt, Re_3Rh, Re_3Ir, and Re_3Co. This is consistent with the results found in this work, in which these systems were found to have large negative heats of mixing. Another HCP-based superstructure, B19, is identified as a ground in the Re-Os system, for which we also find a negative heat of mixing.

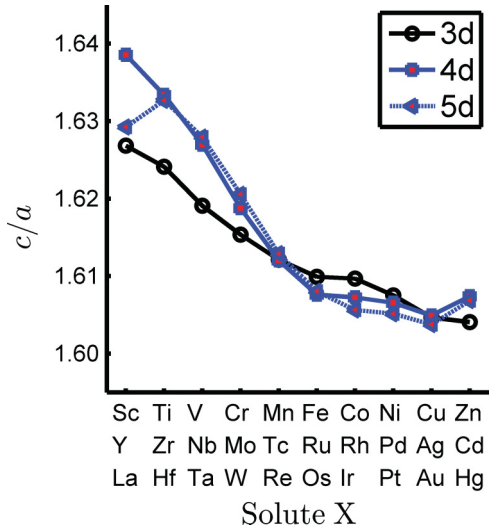

FIG. 2. (Color online) Variation in c/a as a function of $3d$, $4d$, or $5d$ solute element for alloy composition $Re_{15}X_1$.

Published CALPHAD models for the Re-W and Re-Ta system[51] feature negative excess Gibbs energies for both the Re-Ta and Re-W HCP phases. The mixing energy computed in the present work for Re-W with composition $Re_{15}W_1$ is -2.86 kJ/mol, which compares reasonably well to the value of -7.986 kJ/mol from the assessment in Ref. 51. For Re-Ta, however, the published free-energy model predicts a mixing energy of -31.286 kJ/mol for $Re_{15}Ta_1$ composition, which is in sharp contrast to the present calculated value of $+4.85$ kJ/mol.

D. Elastic properties of Re-based transition-metal alloys

Figure 4 plots the calculated values of K, G, and the intrinsic ductility parameter $D = K/G$ for Re-X TM alloys as a function of the number of d electrons for the solutes (X). Both K and G are shown to display concave and roughly parabolic trends, with maximum values occurring in the Fe/Ru/Os column for K and in the Co/Rh/Ir column for G. The K/G ratio displays a convex and roughly parabolic dependence on solute d electron count, with a minimum in the Co/Rh/Ir column. Since higher values of K/G correlate with higher intrinsic ductility, the results in Fig. 4(c) suggest

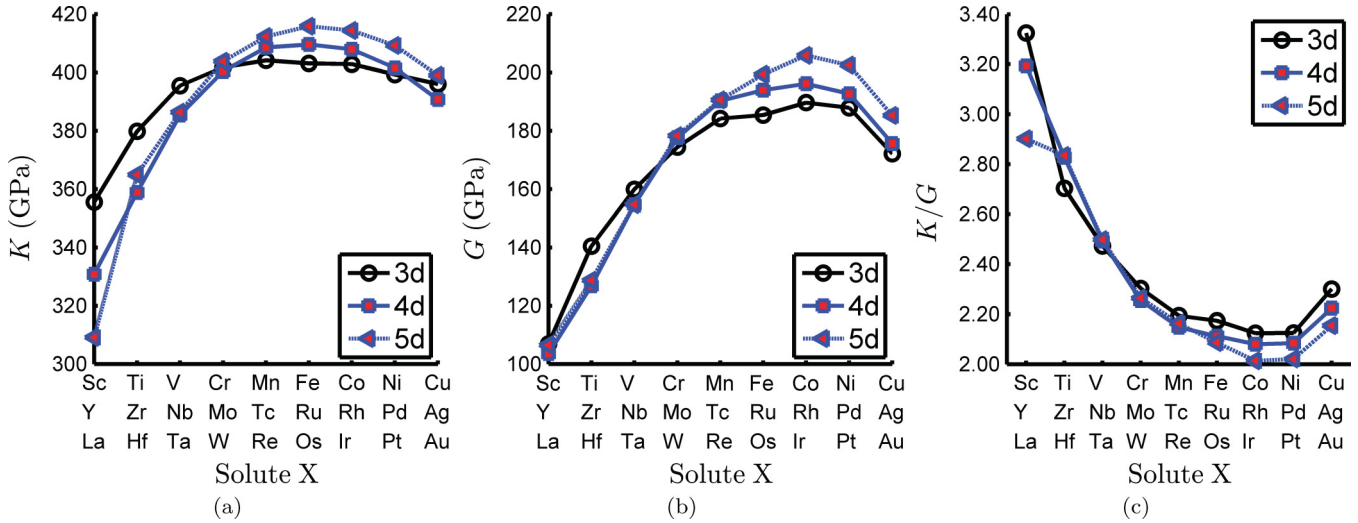

FIG. 4. (Color online) Variation of (a) K, (b) G, and (c) K/G as a function of $3d$, $4d$, or $5d$ solute element for alloy composition $Re_{15}X_1$.

that the addition of solutes to the left or right of Re in the periodic table should increase and decrease the intrinsic ductility, respectively. It is interesting to note that this trend is qualitatively similar to that displayed by the axial c/a ratio in Fig. 2. A table listing calculated values for all of the independent symmetrized elastic constants of the Re-X TM alloys studied in this work is included in the Supplemental Material.[52]

Trends in the elastic anisotropy are shown in Fig. 5, which plots one minus the anisotropy parameters f_E and f_G for the Young's modulus and shear modulus, respectively, as defined in Eqs. (4) and (5). An isotropic material corresponds to f_E and f_G values of one, so that deviations from zero for $1 - f_G$ and $1 - f_E$ in Fig. 5 measure the degree of elastic anisotropy. Alloying of Re with neighboring elements to the left and right in the periodic table are seen to decrease slightly the degree of anisotropy in the Young's modulus. Alloying with elements at the end of the TM series increase the anisotropy in f_E, while the elements Sc, Y, and La, on the left of the TM series, show a considerable scatter in f_E. The effects of alloying on f_G are seen to be weaker overall, relative to f_E. The anisotropy in the shear modulus is seen to be lowest for pure Re, and alloys with its isoelectronic solute elements; alloying with elements to the right or left are seen to weakly increase the magnitude of the deviation of f_G from unity.

IV. DISCUSSION

The DFT-calculated properties for $Re_{15}X_1$ alloys presented in the previous section are shown to display pronounced trends with the number of d electrons in the TM solute atoms X. In this

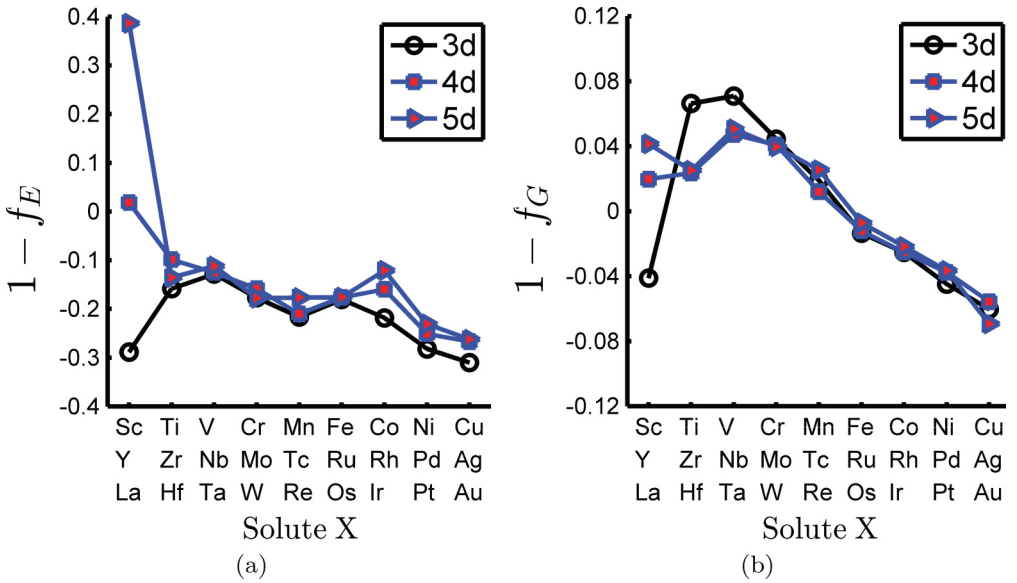

FIG. 5. (Color online) Variation of the elastic anisotropy parameters f_E (a) and f_G (b) as a function of $3d$, $4d$, or $5d$ solute element for alloy composition $Re_{15}X_1$.

section we examine these trends further within the framework of canonical d-band theory.

We consider first the variation in the solute volume expansion coefficient, which is shown to display a parabolic-like variation with band filling in Fig. 1 for each of the $3d$, $4d$, and $5d$ periods. This can be explained readily from the well-known trends in the atomic volumes in the elemental transition metals in their respective equilibrium structures, which vary approximately parabolically with band filling.[53–55] Given that the alloys considered in the present work are substitutional and dilute in nature, Vegards's law (i.e., atomic volume of an alloy varying linearly with concentration) is expected to be a reasonable assumption, such that alloying with solutes with sizes increasingly larger (smaller) than Re should lead to increasingly larger increases (decreases) in the atomic volume of the alloy.

We consider next the calculated trend in the axial c/a ratio, which is shown in Fig. 2 to decrease almost monotonically with the number of d electrons for the solute atoms. In tight-binding, canonical d-band models of the electronic structure of HCP transition metals[56–59] the bond order between neighbors within and out of the basal plane is decomposed into $dd\sigma$, $dd\pi$, and $dd\delta$ two-center hopping-integral contributions. Bonding contributions between neighbors in the basal plane and out of the basal plane are denoted by σ_1,π_1,δ_1 and σ_2,π_2,δ_2, respectively. Starting at half band filling, the σ_1 and σ_2 bonding weakens with a decrease in the number of d electrons, whereas the in-plane bonding π_1 is enhanced while the π_2 bonding levels off (the δ bonding is relatively insignificant).[56] This implies that the bonding in the basal plane gets reinforced with respect to the bonding out of the basal plane with decreasing band filling, which is qualitatively consistent with our finding that the c/a ratio of Re increases when alloyed with TM solutes to the left in the periodic table. Additionally, the π_1 and π_2 bond orders cross at almost exactly the band filling of Re. Consequently, as the band filling is increased, starting from this crossover point, the π_2 bonding starts dominating over π_1, which is expected to lead to the contraction of the c direction relative to the in-plane lattice spacing (a). This is consistent with the present results, which show a decrease in c/a ratio when Re is alloyed with solutes to the right in the periodic table.

Trends in the elastic constants of the pure transition metals in their equilibrium structures with band filling have been fairly well established.[60] Bulk moduli K of the $3d$, $4d$, and $5d$ transition metals have been predicted using canonical d-band theory by Pettifor[58] and these trends have been confirmed by other authors (e.g., Rose and Shore[61]). In transition metals, the general trend is for the bulk modulus to reach a maximum at approximately the Re or Os column of the periodic table. More specifically, for the $5d$ elements, the maximum bulk modulus seems to occur at band filling slightly higher than Re. Near the maximum, the behavior of the bulk modulus with band filling is approximately parabolic. On the other hand, both the Voigt average G and the Reuss average of the shear modulus of the elemental transition metals are known to exhibit different behavior with band filling.[62] Specifically, for the elemental $5d$ transition metals, it is known that G increases almost linearly, varying by about 40% with increasing band filling from W to Re to Os and finally to Ir. Since K levels out in the W-Re-Os band-filling regime, whereas G monotonically increases, these observations are consistent with the present work showing that K/G decreases (increases) when alloying Re with solute atoms to the right (left) in the periodic table.

The variation of the bulk modulus and the Voigt average of the shear modulus of $Re_{15}X_1$ alloys with band filling is shown in Figs. 4(a) and 4(b), respectively. These quantities approximately follow the same trend as those of the pure transition metals with band filling: approximately parabolic behavior with a maximum at higher band filling then Re. Interestingly, the higher ductility parameter from Re-based alloys with lower band filling than Re is not caused by an increase of K and a decrease of G, as one might expect but merely by a relatively lower decrease in G compared to K for lower band filling than Re. For example, the Re-based Re-La alloy has a value for K which is about 25% lower than for Re, whereas G decreases by nearly 50%, yielding an increase of the ductility parameter.

Canonical d-band theory can be used to outline the trends in the energetics of Re-based alloys as follows. Within this framework, the enthalpy of formation of a transition metal alloy from the pure elements can be decomposed into four physically distinct parts:[6] i) a contribution from the transfer of electrons to equalize the Fermi level, which is always negative, ii) a contribution that stems from the difference in Density of States (DOS) bandwidth of the pure elements, which can be either positive or negative, iii) a contribution that comes from the change of shape of the DOS when alloying, and iv) a contribution that comes from Coulomb energy due to charge transfer. In the simplest model, only the first two contributions are taken into account. Continuing along these lines, the heat of formation for a binary transition metal alloy A_xB_{1-x} can be expressed[63] as in Eq. (9),

$$E_{\text{form}} = -\frac{Z_d(1-Z_d/10)}{2}W_d + x\frac{Z_{dA}(1-Z_{dA}/10)}{2}W_{dA} + (1-x)\frac{Z_{dB}(1-Z_{dB}/10)}{2}W_{dB}. \quad (9)$$

The DOS bandwidth of the alloy A_xB_{1-x} is denoted by W_d, whereas the DOS bandwidths for the pure elements A and B are

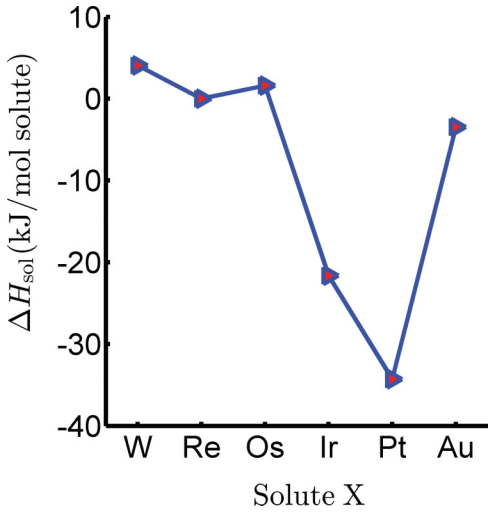

FIG. 6. (Color online) Canonical d-band heat of solution as a function of various $5d$ solute elements for alloy composition $Re_{15}X_1$.

given by W_{dA} and W_{dB}, respectively. The number of electrons in the d band for the alloy and elements A and B is given by Z_d, Z_{dA}, and Z_{dB}, respectively.

The parameters appearing in Eq. (9) can be computed from DFT calculations. However, for the purposes of the present qualitative analysis we use the published muffin-tin-orbital values for transition metals[63] to compare with the trends shown in Fig. 3. Using the theory outlined above, based on canonical d-band theory, we have obtained the heat of solution for various Re-based 5d transition metal alloys shown in Fig. 6. Comparing the DFT-calculated heat of solution from Fig. 3 to the quantities computed from canonical d-band theory in Fig. 6, it is seen that the trends in the heat of solution are predicted correctly. The sign is not predicted consistently with DFT in all cases, although the trends with the deep minimum to the right of Re and the higher values to the left are present. The actual values of the heat of solution are off by factors of between 2 and 5 which is not unreasonable considering the approximations inherent in the model.

V. SUMMARY AND CONCLUSION

In summary, the present work has involved a computational study of the structural, energetic and elastic properties of HCP rhenium-based transition-metal alloys. Trends in the atomic volume, axial c/a ratio, elastic constants and formation energies of $Re_{15}X_1$ alloys are investigated for all 3d, 4d, and 5d solute species X. Each of the calculated properties show clear trends with band filling that are well described by the d-band theory of transition-metal bonding.

The practical interest in Re-based materials is associated with the combination of their high melting points and good low-temperature ductility. Thus, in the context of the design of lower-cost Re-based alloys the key findings of this work relate to the effects of solute additions on the elastic anisotropy and the intrinsic ductility parameter K/G. It is found that alloying Re with elements to the left in the periodic table increases K/G, and is thus expected to enhance the intrinsic ductility. The trend in K/G correlates with an increase in the axial c/a ratio, towards values closer to ideal close packing, when alloying with solutes that decrease the average band filling. The effect of alloying on the elastic anisotropy is examined by considering two parameters that measure the anisotropy of the Young's modulus and shear modulus. As described in the first section of the paper, it is expected generally that an increase in the elastic anisotropy could contribute to brittle behavior in polycrystalline samples. In the present calculations alloying with solute additions near Re in the periodic table is found to weakly decrease (increase) the anisotropy in Young's modulus (shear modulus).

ACKNOWLEDGMENTS

The authors would like to thank John W. Morris, Jr., for helpful discussions, and the US Office of Naval Research for their financial support of this project under Grant No. N00014-11-1-0886. This work made use of computational resources provided under the Extreme Science and Engineering Discovery Environment (XSEDE), which is supported by National Science Foundation Grant No. OCI-1053575.

*maartendft@berkeley.edu

[1] J. Carlen and B. Bryskin, Mater. Manuf. Processes **9**, 1087 (1994).
[2] I. Campbell, D. Rosenbaum, and B. Gonser, J. Less-Common Met. **1**, 185 (1959).
[3] A. Wrona, M. Staszewski, M. Czepelak, M. Woch, M. Kamińska, M. Osadnik, and D. Kołacz, Arch. Mater. Sci. **45**, 95 (2010).
[4] P. Fink, J. Miller, and D. Konitzer, JOM **62**, 55 (2010).
[5] S. Shang, D. Kim, C. Zacherl, Y. Wang, Y. Du, and Z. Liu, J. Appl. Phys. **112**, 053515 (2012).
[6] M. Cyrot and F. Cyrot-Lackmann, J. Phys. F **6**, 2257 (1976).
[7] F. Cyrot-Lackmann, J. Phys. Chem. Solids **29**, 1235 (1968).
[8] J. Friedel, in *Physics of Metals*, edited by J. Ziman (Cambridge University Press, New York, 1969); Solid State Phys. **40**, 43 (1969).
[9] M. Yoo, Metall. Mater. Trans. A **12**, 409 (1981).
[10] U. V. Waghmare, E. Kaxiras, and M. S. Duesbery, Physica Status Solidi(b) **217**, 545 (2000).
[11] N. Bernstein and E. B. Tadmor, Phys. Rev. B **69**, 094116 (2004).
[12] M. Yoo, J. Morris, K. Ho, and S. Agnew, Metall. Mater. Trans. A **33**, 813 (2002).
[13] D. Bacon and V. Vitek, Metall. Mater. Trans. A **33**, 721 (2002).
[14] M. J. Mehl, D. A. Papaconstantopoulos, N. Kioussis, and M. Herbranson, Phys. Rev. B **61**, 4894 (2000).
[15] J. R. Rice, J. Mech. Phys. Solids **40**, 239 (1992).
[16] M. Yoo, Oak Ridge National Laboratory, Report No. CONF-9106146-1, 1991 (unpublished).
[17] P. Gumbsch, Mater. Sci. Eng. A **319**, 1 (2001).
[18] A. Fallahi and A. Ataee, Mater. Sci. Eng. A **527**, 4576 (2010).
[19] D. Tromans, Int. J. Res. Rev. Appl. Sci. **6**, 462 (2011).
[20] A. Churchman, Trans. AIME **218**, 262 (1960).
[21] G. Geach, R. JEFFERY, and E. Smith, in *Rhenium: Papers Presented at the Symposium on Rhenium of the Electrothermics and Metallurgy Division of the Electrochemical Society, May 3 and 4, 1960, Chicago, Illinois* (Elsevier, Amsterdam, 1962), p. 84.
[22] R. Jeffery and E. Smith, Philos. Mag. **13**, 1163 (1966).
[23] P. E. Blöchl, Phys. Rev. B **50**, 17953 (1994).
[24] G. Kresse and D. Joubert, Phys. Rev. B **59**, 1758 (1999).
[25] G. Kresse and J. Furthmüller, Phys. Rev. B **54**, 11169 (1996).
[26] G. Kresse and J. Hafner, Phys. Rev. B **47**, 558 (1993).
[27] D. M. Ceperley and B. J. Alder, Phys. Rev. Lett. **45**, 566 (1980).
[28] J. P. Perdew and A. Zunger, Phys. Rev. B **23**, 5048 (1981).
[29] H. J. Monkhorst and J. D. Pack, Phys. Rev. B **13**, 5188 (1976).
[30] M. Methfessel and A. T. Paxton, Phys. Rev. B **40**, 3616 (1989).
[31] M. Moakher and A. Norris, J. Elast. **85**, 215 (2006).
[32] F. Tasnádi, M. Odén, and I. A. Abrikosov, Phys. Rev. B **85**, 144112 (2012).
[33] J. Browaeys and S. Chevrot, Geophys. J. Int. **159**, 667 (2004).
[34] G. Simmons and H. Wang, *Single Crystal Elastic Constants and Calculated Aggregate Properties* (MIT Press, Cambridge, 1971).
[35] M. Methfessel, C. O. Rodriguez, and O. K. Andersen, Phys. Rev. B **40**, 2009 (1989).

[36]M.-B. Lv, Y. Cheng, Y.-Y. Qi, G.-F. Ji, and C.-G. Piao, Physica B: Condensed Matter **407**, 778 (2012).
[37]G. Steinle-Neumann, L. Stixrude, and R. E. Cohen, Phys. Rev. B **60**, 791 (1999).
[38]S. Vosko, L. Wilk, and M. Nusair, Can. J. Phys. **58**, 1200 (1980).
[39]L. Hedin and B. Lundqvist, J. Phys. C **4**, 2064 (1971).
[40]J. P. Perdew, K. Burke, and M. Ernzerhof, Phys. Rev. Lett. **77**, 3865 (1996).
[41]D. R. Hamann, M. Schlüter, and C. Chiang, Phys. Rev. Lett. **43**, 1494 (1979).
[42]L. Fast, J. M. Wills, B. Johansson, and O. Eriksson, Phys. Rev. B **51**, 17431 (1995).
[43]E. Wimmer, H. Krakauer, M. Weinert, and A. J. Freeman, Phys. Rev. B **24**, 864 (1981).
[44]Y. K. Vohra, S. J. Duclos, and A. L. Ruoff, Phys. Rev. B **36**, 9790 (1987).
[45]L. Liu, T. Takahashi, and W. Bassett, J. Phys. Chem. Solids **31**, 1345 (1970).
[46]T. S. Duffy, G. Shen, D. L. Heinz, J. Shu, Y. Ma, H. K. Mao, R. J. Hemley, and A. K. Singh, Phys. Rev. B **60**, 15063 (1999).
[47]M. Manghnani, K. Katahara, and E. Fisher, Phys. Rev. B **9**, 1421 (1974).
[48]P. S. Rudman, J. Less-Common Met. **12**, 79 (1967).
[49]M. Jahnátek, O. Levy, G. L. W. Hart, L. J. Nelson, R. V. Chepulskii, J. Xue, and S. Curtarolo, Phys. Rev. B **84**, 214110 (2011).
[50]O. Levy, M. Jahnátek, R. V. Chepulskii, G. L. W. Hart, and S. Curtarolo, J. Am. Chem. Soc. **133**, 158 (2011).
[51]Z. Liu and Y. Chang, J. Alloys Compd. **299**, 153 (2000).
[52]See Supplemental Material at http://link.aps.org/supplemental/10.1103/PhysRevB.86.224101 for a table listing all the independent elastic constants calculated for Re-*X* TM alloys.
[53]T. Qin, R. Drautz, and D. G. Pettifor, Phys. Rev. B **78**, 214108 (2008).
[54]J. A. Moriarty and M. Widom, Phys. Rev. B **56**, 7905 (1997).
[55]V. Ozoliņš and M. Körling, Phys. Rev. B **48**, 18304 (1993).
[56]A. Sutton, M. Finnis, D. Pettifor, and Y. Ohta, J. Phys. C **21**, 35 (1988).
[57]M. Finnis, A. Paxton, D. Pettifor, A. Sutton, and Y. Ohta, Philos. Mag. A **58**, 143 (1988).
[58]D. Pettifor and R. Podloucky, J. Phys. C **19**, 315 (1986).
[59]D. Pettifor, J. Phys. F **7**, 613 (1977).
[60]J. Wills, O. Eriksson, P. Söderlind, and A. Boring, Phys. Rev. Lett. **68**, 2802 (1992).
[61]J. H. Rose and H. B. Shore, Phys. Rev. B **49**, 11588 (1994).
[62]M. Morinaga, T. Nambu, J. Fukumori, M. Kato, T. Sakaki, Y. Matsumoto, Y. Torisaka, and M. Horihata, J. Mater. Sci. **30**, 1105 (1995).
[63]W. Harrison, *Elementary Electronic Structure* (World Scientific, Singapore, 1999).